IV. Tracking and Navigational Accuracy Analysis

ADVANCED ENGINEERING

A. Introduction, *T. W. Hamilton and B. D. Mulhall*

The DSN Inherent Accuracy Project was formally established by the DSN Executive Committee in July 1965. The objectives of the project are:

(1) Determination (and verification) of the inherent accuracy of the DSN as a radio navigation instrument for lunar and planetary missions.

(2) Formulation of designs and plans for refining this accuracy to its practical limits.

Achievement of these goals is the joint responsibility of the Telecommunications and Mission Analysis Divisions of JPL. To this end, regular monthly meetings are held to coordinate and initiate relevant activities. The project leader and his assistant (from the Mission Analysis and Telecommunications Divisions, respectively) report to the DSN Executive Committee, and are authorized to task project members to (1) conduct analyses of proposed experiments, (2) prepare reports on current work, and (3) write descriptions of proposed experiments. The project is further authorized to deal directly with those flight projects using the DSN regarding data-gathering procedures that bear on inherent accuracy.

The various data types and tracking modes provided by the DSIF in support of lunar and planetary missions are discussed in SPS 37-39, Vol. III, pp. 6–8. Technical work directly related to the Inherent Accuracy Project is presented in SPS 37-38, Vol. III, and in subsequent *Deep Space Network* SPS volumes, and is continued in the following sections of this volume.

For most upcoming planetary missions, such as *Mariner* Mars 1971, the tightest bounds on the allowable errors for a number of parameters arise from the navigational accuracy requirements during encounter support. In particular, encounter navigational accuracy is most sensitive to error sources that cause a diurnal signature on the radio tracking data (SPS 37-39, Vol. III, pp. 18–24). These sources of error are of two classes: (1) those parameters that define the locations of the DSS in inertial space, and (2) those phenomena that directly affect the DSS tracking data. The first category includes the locations of the DSS with respect to earth's crust; Universal Time (UT1); polar motion (the motion of the earth's crust with respect to the spin axis); precession and nutation (orientation of the earth's spin axis with respect to inertial space); and the ephemerides of the earth, moon, and target body. Of these, uncertainties in the first three are currently the

major limitations to the encounter support of navigation accuracy.

The dominant sources of error in the second category are those affecting the tracking data directly. These include frequency system instability, electrical phase path variations (through both the spacecraft and the DSS), and the transmission media (the troposphere and the charged particles in the ionosphere and space plasma).

The two articles in this chapter are concerned with the effects of the transmission media on DSN navigational accuracy. The first article, *Section B,* concentrates on tropospheric effects on navigation errors. This article discusses the temporal variation of tropospheric errors as measured by radiosonde balloon data. A cursory examination of surface weather measurements as a calibration technique and their correlations with the zenith range effect is also discussed.

The second article, *Section C,* deals with the effects of the earth's ionosphere on tracking data. The sensitivity of navigation errors to the ionospheres for differences in seasons, solar cycle, and mission geometries (inner vs outer planet missions) is described.

In the investigation of transmission media effects on navigation, the need for data not normally collected by the DSN has arisen. Consequently, the Jet Propulsion Laboratory has worked with outside agencies in obtaining and exchanging atmospheric data. Examples of this are the studies discussed in *Sections B* and *C*. The radiosonde data used in tropospheric studies were obtained from the National Bureau of Standards. The ionospheric data used in the study discussed in *Section C* were obtained from the Center for Radar Astronomy, Stanford Electronics Laboratories, and from devices installed at the Goldstone DSCC. Through Stanford's cooperation with JPL, a Faraday rotation polarimeter designed and built by Stanford is currently on loan to JPL and is being used to monitor the ATS-1 satellite to obtain ionospheric calibration data for the Goldstone complex.

B. Variations in the Zenith Tropospheric Range Effect Computed From Radiosonde Balloon Data, *V. J. Ondrasik and K. L. Thuleen*

1. Introduction

For many years it has been recognized that the passage of a tracking signal through the troposphere will significantly corrupt the data used in determining the orbit of a distant spacecraft. At the present time (July 1970), a tropospheric refractivity model, which is independent of time, is being used in attempts to reduce the tropospheric errors. Some idea of the temporal behavior of errors in radio tracking data due to the troposphere is obtained by calculating the tropospheric zenith range effect from measured refractivity profiles collected during 1967. In addition, a cursory examination of the surface weather measurements is undertaken to see if it may be worthwhile to try to predict the zenith range effect from such measurements.

2. Zenith Range Effect

It is convenient to think of the range measurement ρ, divided by c, as the time it takes a radio signal to travel from the spacecraft to the tracking station. This concept is expressed by

$$\rho = c \int_{\text{path}} \frac{ds}{v(s)} \tag{1}$$

where

ds = an element of the ray path over which the signal travels

$v(s)$ = the velocity of the radio signal on the path

c = the velocity of light in a vacuum

In general the presence of the troposphere will cause the path to curve, as well as retarding the velocity of the radio

signal. However, when the spacecraft is at the zenith, there will be no bending and Eq. (1) reduces to

$$\rho_z = \rho\,(\text{zenith}) = \int_0^\infty \frac{c}{v(h)}\,dh \tag{2}$$

where h is the height above the station. By definition

$$n = \frac{c}{v} = 1 + N \times 10^{-6} \tag{3}$$

where

n = index of refraction

N = refractivity

Clearly, then, the zenith range effect $\Delta\rho_z$, which is the difference between the measured and geometric ranges to an object at the zenith, is given by

$$\Delta\rho_z = \rho_z - \rho_z\,(\text{geo.}, v = c) = 10^{-6}\int_0^\infty N(h)\,dh \tag{4}$$

Thus, once the refractivity profile $N(h)$ is known, $\Delta\rho_z$ may be calculated from Eq. (4).

3. Tropospheric Refractivity Profile

The refractivity of the troposphere is commonly determined from the following equation (Ref. 1):

$$N = \frac{77.6}{T'}\left(P + \frac{4810e}{T'}\right) \tag{5}$$

where

P = pressure, mb

T' = temperature, °K

e = vapor pressure, mb

and

$$e = \left[6.1 \times \exp_{10}\left(\frac{7.4475T}{234.7 + T}\right)\right] \times \frac{R}{100}$$

where

R = relative humidity, %

T = temperature, °C

$\exp_{10} y = 10^y$

The first and second terms of N will be referred to as the dry and wet refractivities, respectively. An approximation to the errors in N resulting from the use of Eq. (5), due both to the errors in the equation itself and to errors in the meterological measurement(s), is given by Bean and Dutton (Ref. 1), and is summarized in Table 1.

Table 1. Errors in the equation for refractivity

Error source	Ratio of rms error in refractivity to refractivity[a]
Equation (5)	0.5%
Surface weather observations (±1 mb, ±0.1 °C, ±1% R)	0.2%
Radiosone observations (±2 mb, ±1 °C, ±5% R)	1.3%

[a] p = 1013 mb, T = 15 °C, R = 60%.

Presently the best source of obtaining the necessary weather measurements to determine the refractivity profile (i.e., N versus h) from Eq. (5) is by using radiosonde balloon observations. The data which are generally retained from these observations are the pressure, temperature, and humidity at both the standard pressure levels and at any pressure level where the observer notices any significant changes in the data from a nominal. An example of this type of data is shown in Table 2. Generally the overseas data are not as complete and terminate at approximately 350 mb.

A determination of the height above sea level corresponding to the standard and significant pressure levels may be found by using the hydrostatic equation and a particular gas law. The computation of the heights in this way and an interpolation between the resulting points to obtain the pressure, temperature, vapor pressure, and relative humidity at the surface and every 1000 ft above mean sea level is done in the program CNVTWR. This program is a slight modification of the program AFFTC which is used at Edwards AFB and was supplied by Capt. G. Fredricks, U.S. Air Force, 6th Weather Wing. An abbreviated example of the output of CNVTWR is given in columns 2 through 6 of Table 3.

These sets of the pressure temperature and vapor pressure for every 1000 ft of altitude may be substituted into Eq. (5) to give the corresponding total, dry, and wet refractivities. The calculations for determining the refractivity profiles in this manner were performed and an

abbreviated example is given in the seventh, eighth, and ninth columns of Table 3.

4. Calculation of the Zenith Range Effect

According to Eq. (4) the zenith range effect may be written as

$$\Delta\rho_z \doteq 10^{-6}\int_0^\infty N(h)\,dh \tag{6}$$

To accommodate the results of the previous section, the above integral is replaced by the following summation:

$$\Delta\rho_z = \sum_{i=1}\Delta\rho_i \tag{7}$$

where

$$\Delta\rho_i = 10^{-6}\int_{h_{i-1}}^{h_i} N(h)\,dh \tag{8}$$

and i is the index of the refractivity profile table. Before the integral in Eq. (8) can be integrated, it is necessary to specify $N(h)$. This study calculates $\Delta\rho_i$ by assuming that $N(h)$ assumes the tabular values N_{i-1} and N_i at h_{i-1} and h_i, respectively, and has an exponential behavior with inverse scale height, B_i, between these two heights. For this type of atmosphere, Eq. (8) may be written as

$$\Delta\rho_i = 10^{-6}\frac{1}{B_i}\left(N_{i-1} - N_i\right) \tag{9}$$

where

$$B_i = \frac{\ln\left[N(h_{i-1})\right] - \ln\left[N(h_i)\right]}{h_i - h_{i-1}} \tag{10}$$

An example of the zenith range effect and inverse scale heights computed according to Eqs. (7–10) is given in the last nine columns of Table 3.

5. Data

To determine what type of values the zenith range effect may assume, weather data profiles for 1967 were obtained from the radiosonde balloon data site nearest to each of the tracking stations. The Edwards AFB data was supplied by Capt. G. Fredricks and the overseas data was obtained from the National Weather Records Center in Asheville, N. C., in cooperation with Mr. Wayne Hensley and Mr. Richard Davis of that agency.

Table 2. Standard and significant pressure level radiosonde balloon data observed at Edwards AFB, August 2, 1968

Standard pressure level data			Significant pressure level data		
Pressure, mb	Temperature, °C	Relative humidity, %	Pressure, mb	Temperature, °C	Relative humidity, %
931.2[a]	19.0	49.7	931.2[a]	19.0	49.7
900.0	23.5	46.3	920.0	23.2	48.5
850.0	22.2	42.9	880.0	23.9	44.1
800.0	19.2	41.3	802.0	19.4	40.9
750.0	13.9	51.7	709.0	9.4	60.7
700.0	8.9	58.0	625.0	5.3	33.4
650.0	6.5	41.9	454.0	−10.3	35.2
600.0	3.3	33.7	400.0	−19.0	36.0
550.0	−1.0	34.2	289.0	−39.5	36.5
500.0	−5.6	34.7	233.0	−51.7	9.0[b]
450.0	−10.9	35.3	163.0	−63.0	9.0[b]
400.0	−19.0	35.0	112.0	−68.6	9.0[b]
350.0	−27.4	36.2	100.0	−66.5	9.0[b]
300.0	−37.2	36.4	86.0	−68.6	9.0[b]
250.0	−47.7	18.0	70.0	−60.4	9.0[b]
200.0	−56.5	9.0[b]	23.0	−49.7	9.0[b]
175.0	−60.7	9.0[b]	10.0	−37.9	9.0[b]
150.0	−64.2	9.0[b]	8.0	−40.0	9.0[b]
125.0	−66.9	9.0[b]	4.0	−26.1	9.0[b]
80.0	−65.7	9.0[b]			
70.0	−60.4	9.0[b]			
60.0	−59.0	9.0[b]			
50.0	−57.2	9.0[b]			
40.0	−55.1	9.0[b]			
30.0	−52.3	9.0[b]			
25.0	−50.5	9.0[b]			
20.0	−47.8	9.0[b]			
15.0	−43.7	9.0[b]			
10.0	−37.9	9.0[b]			
7.0	−37.3	9.0[b]			
5.0	−30.6	9.0[b]			
4.0	−26.1	9.0[b]			

[a]Surface.

[b]Calculated values.

Table 4 lists the location of the radiosonde balloon sites, the distance from the nearest tracking station, and the elevation of the tracking station.

Generally the overseas data went up to only 30,000 ft while the Edwards AFB data usually went above 80,000 ft.

Table 3. Weather measurements, refractivities, zenith range effect, and inverse scale heights as a function of altitude for radiosonde balloon observations at Edwards AFB on May 24, 1967

Index	Altitude, ft	Pressure, mb	Temperature, °C	Vapor pressure, mb	Relative humidity, %	Refractivity			Zenith range effect from surface, m			Inverse exponential scale height, km^{-1}		
						Total	Dry	Wet	Total	Dry	Wet	Total	Dry	Wet
0	2375	927.2	24.0	7.5	25	273.8	242.1	31.7	—	—	—	—	—	—
1	3000	907.2	24.2	7.6	25	268.8	236.8	32.1	0.052	0.046	0.006	0.097	0.118	−0.062
2	4000	876.1	23.5	7.4	25	260.5	229.2	31.4	0.132	0.117	0.016	0.103	0.107	0.072
3	5000	845.9	21.6	6.8	26	251.9	222.7	29.2	0.210	0.185	0.025	0.111	0.094	0.235
4	6000	816.6	19.6	6.2	27	243.4	216.5	27.0	0.286	0.252	0.034	0.112	0.093	0.258
5	7000	788.1	17.5	5.7	28	235.6	210.4	25.2	0.359	0.317	0.041	0.108	0.093	0.229
6	8000	760.3	14.9	5.8	34	230.9	204.8	26.1	0.430	0.381	0.049	0.066	0.088	−0.116
7	9000	733.3	12.2	5.7	40	225.5	199.4	26.1	0.500	0.442	0.057	0.077	0.088	−0.005
8	10000	707.0	9.6	5.4	45	219.2	194.0	25.2	0.567	0.502	0.065	0.093	0.090	0.117
10	12000	656.7	5.2	3.6	41	200.4	183.1	17.3	0.695	0.617	0.078	0.135	0.095	0.529
12	14000	609.0	−0.7	3.2	56	189.5	173.5	16.1	0.814	0.726	0.088	0.093	0.089	0.129
14	16000	564.0	−5.1	2.9	71	178.3	163.3	15.1	0.926	0.828	0.097	0.107	0.101	0.168
16	18000	521.6	−9.7	2.5	85	167.1	153.6	13.4	1.031	0.925	0.106	0.108	0.100	0.195
18	20000	481.8	−14.4	1.7	85	154.0	144.5	9.5	1.129	1.016	0.113	0.148	0.102	0.788
23	25000	392.9	−23.4	0.7	73	126.3	122.1	4.2	1.340	1.218	0.121	0.123	0.114	0.394
28	30000	317.4	−36.7	0.2	61	105.5	104.2	1.3	1.516	1.390	0.125	0.103	0.105	−0.077
33	35000	253.2	−49.3	0	43	87.8	87.8	0	1.663	1.537	0.126	0.133	0.133	—
38	40000	199.6	−60.6	0	12	72.9	72.9	0	1.785	1.659	0.126	0.124	0.124	—
43	45000	156.1	−61.4	0	9	57.2	57.2	0	1.884	1.758	0.126	0.179	0.179	—
48	50000	122.4	−61.8	0	9	44.9	44.9	0	1.962	1.836	0.126	0.165	0.165	—
58	60000	74.7	−62.4	0	9	27.5	27.5	0	2.070	1.944	0.126	0.166	0.166	—
68	70000	45.9	−57.3	0	9	16.5	16.5	0	2.136	2.010	0.126	0.171	0.171	—
78	80000	28.6	−52.2	0	9	10.0	10.0	0	2.175	2.050	0.126	0.158	0.158	—
88	90000	18.0	−49.2	0	9	6.2	6.2	0	2.200	2.074	0.126	0.156	0.156	—
98	100000	11.4	−44.3	0	9	3.9	3.9	0	2.215	2.089	0.126	0.144	0.144	—
108	110000	7.3	−39.0	0	9	2.4	2.4	0	2.224	2.089	0.126	0.136	0.136	—
118	120000	4.7	−35.9	0	9	1.5	1.5	0	2.230	2.104	0.126	0.141	0.141	—

Table 4. Radiosonde balloon site parameters

Radiosonde station	Latitude	Longitude	Elevation, m	Nearest DSS	DSS elevation, m	Distance from DSS, km
Edwards AFB	34°55′ N	117°54′ W	724	Goldstone[a]	1032	100
Madrid	40°28′ N	3°34′ W	606	Madrid[b]	789	70
Wagga	35°10′ S	147°28′ E	214	Canberra	656	140
Woomera	31°9′ S	136°48′ E	165	Woomera	151	
Pretoria	25°44′ S	28°11′ E	1330	Johannesburg	1398	50

[a]DSS 14.
[b]DSS 61.

6. Computed Zenith Range Effect

After each month's weather data has been used to calculate the total, dry, and wet zenith range effects from the surface to various altitudes, $\Delta\rho_z$ is plotted as a function of time of the month and the monthly averages and standard deviations are calculated. For example, Fig. 1 shows the daily variations of the zenith range effect produced by the portion of the troposphere between the surface and 80,000 ft over Edwards AFB during March 1967, with the average, the average plus the standard deviation, and the average minus the standard deviation also included. The corresponding values of the total and dry zenith range effects for the total troposphere may be obtained by adding 6 cm to the surface to 80,000-ft level results.

To better illustrate the daily variations in the zenith range effect the difference of the zenith range effects from their monthly averages are also plotted. An example of these deviations is given in Fig. 2, where the average, and the average plus and minus the standard deviation are plotted again.

Similar plots for the overseas stations which would give representative values of the total and dry zenith range effects may not be obtained from the radiosonde balloon data alone because the data usually stops at about 30,000 ft. However, representative values of the complete dry zenith range effect may be found by using the high correlation between this quantity and the surface pressure. This correlation will be illustrated in the next section.

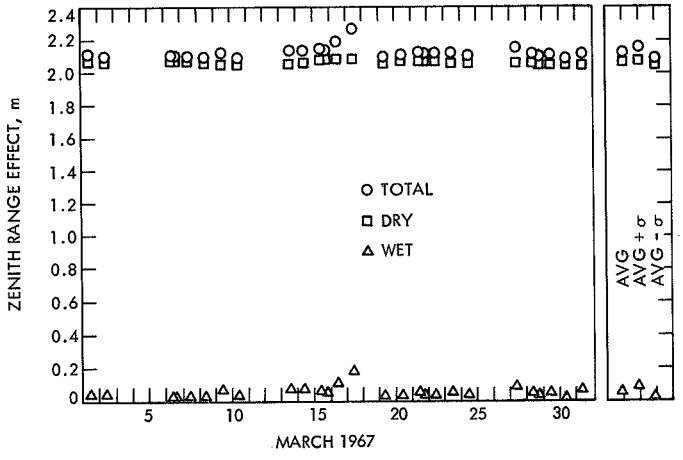

Fig. 1. Total, dry, and wet zenith range effects for portion of troposphere between surface and 80,000 ft over Edwards AFB during March 1967

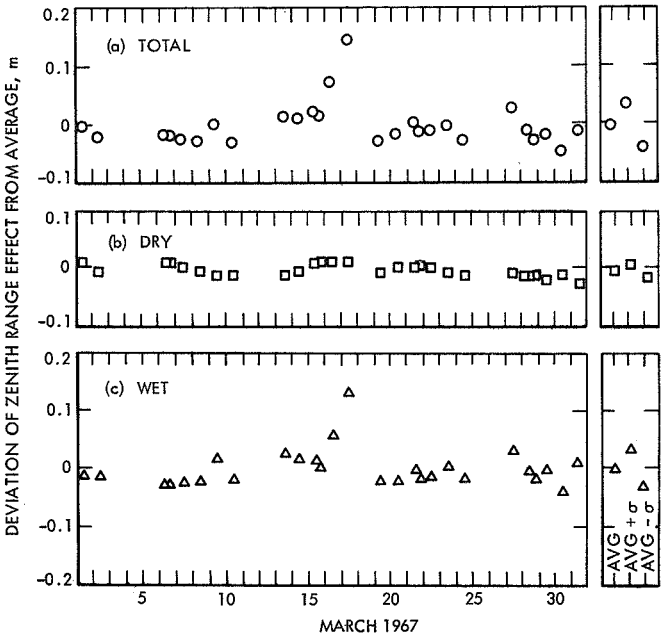

Fig. 2. Deviations from monthly averages of total, dry, and wet zenith range effects over Edwards AFB during March 1967

Figures 3 through 7 summarize the preceding monthly results by plotting for each month the monthly average, the average plus and minus the standard deviation, and the maximum and minimum values of the zenith range effects. These graphs illustrate the important feature that the total zenith range effect seldom varies by more than $\pm 5\%$ from the yearly average.

Figures 3 through 7 also include the zenith range effect obtained by using the profile which currently is used to make tropospheric corrections in the orbit determination program. This profile is exponential in character with a sea level value of 340 and scale height of 7.042 km. The total zenith range effect computed by the following equation agrees to within approximately $\pm 4\%$ of the yearly average computed from the radiosonde balloon data:

$$\Delta\rho_z\,(\text{const exp}) = 340 \times 10^{-6} \int_{x_s}^{\infty} \exp\left[-\frac{x}{7.042}\right] dx$$

where

x_s = height of station above sea level, km

x = height above sea level, km

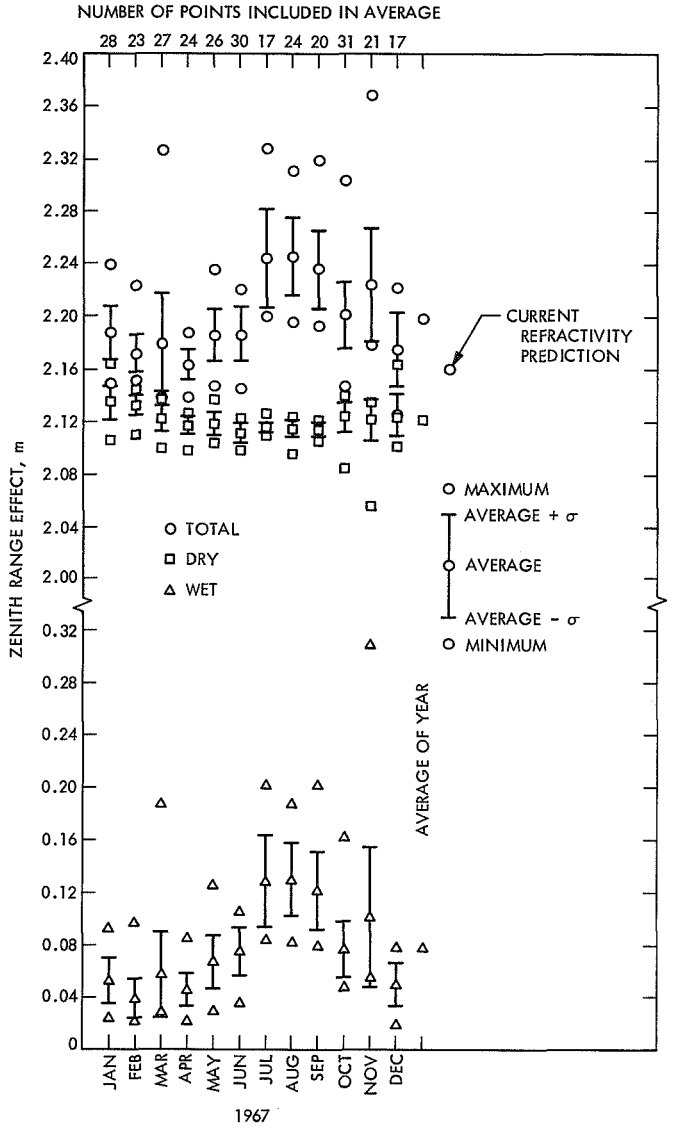

Fig. 3. Monthly averages and standard deviations of total, dry, and wet zenith range effects over Edwards AFB during 1967

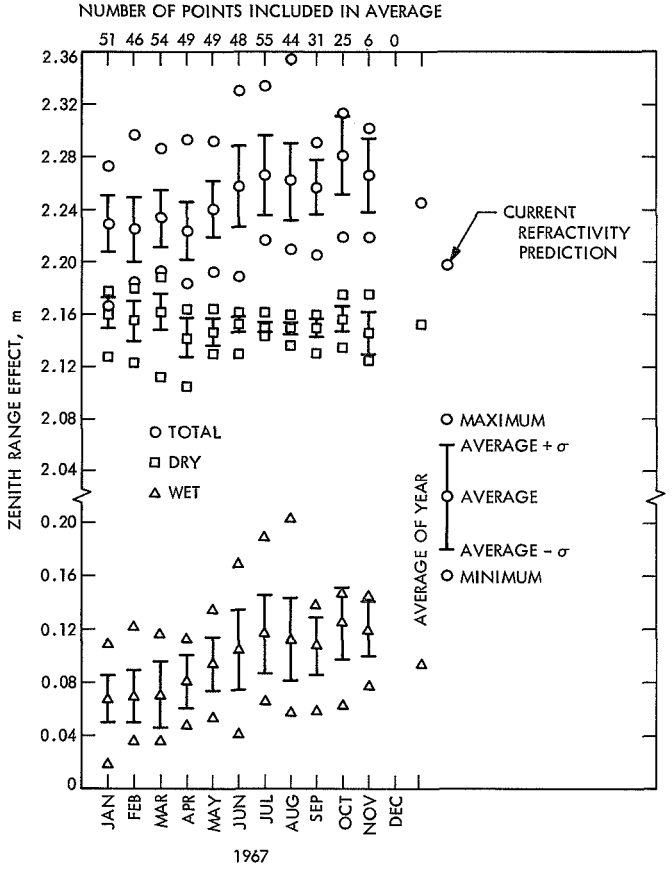

Fig. 4. Monthly averages and standard deviations of total, dry, and wet zenith range effects over Madrid during 1967

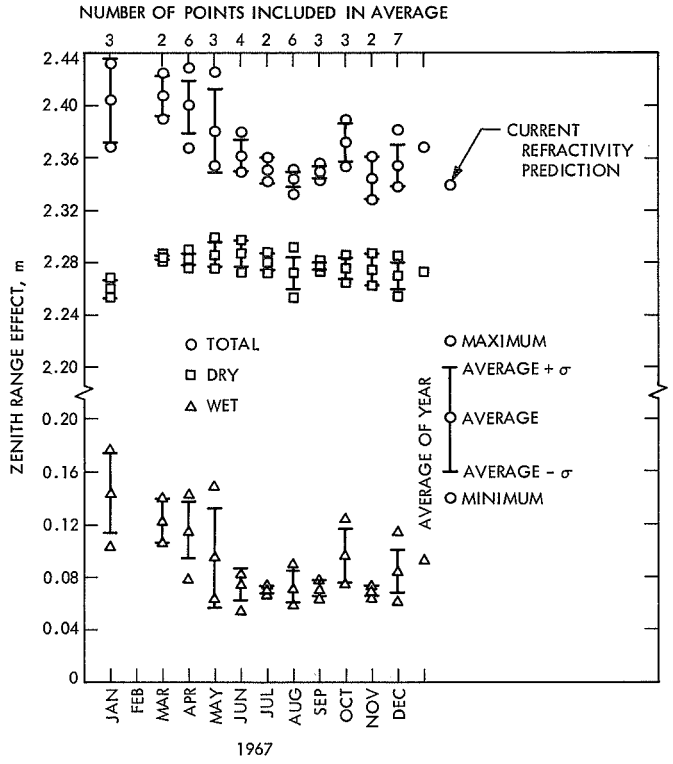

Fig. 5. Monthly averages and standard deviations of total, dry, and wet zenith range effects over Woomera during 1967

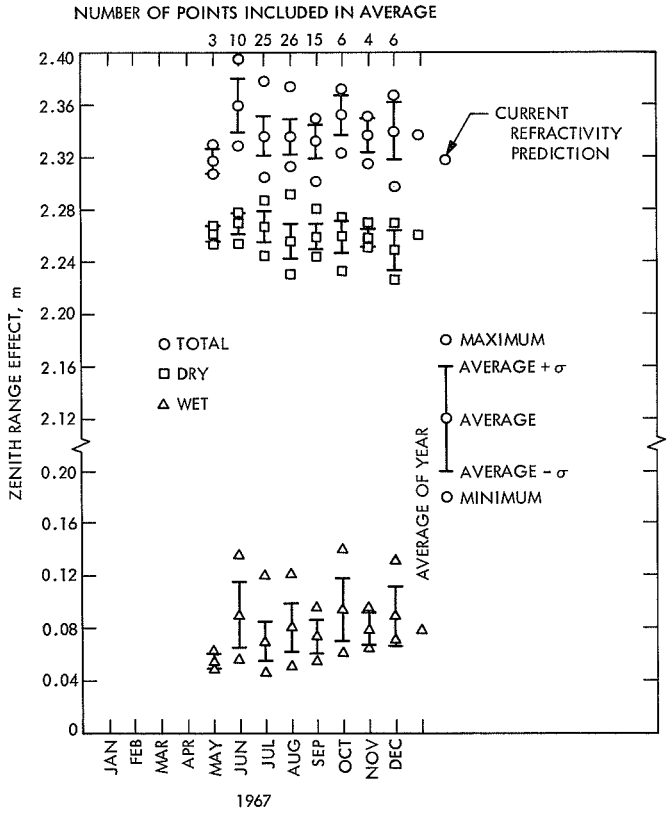

Fig. 6. Monthly averages and standard deviations of total, dry, and wet zenith range effects over Wagga during 1967

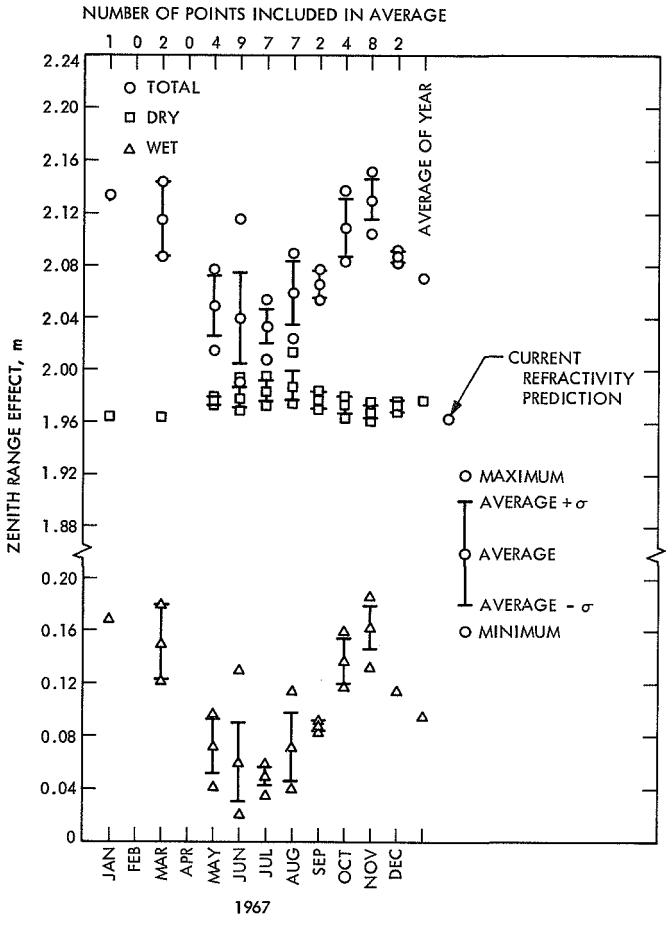

Fig. 7. Monthly averages and standard deviations of total, dry, and wet zenith range effects over Pretoria during 1967

7. Prediction of Dry Zenith Range Effect From the Surface Pressure

From Eqs. (4) and (5), the dry zenith range effect may be written as

$$\Delta\rho_z\,(\text{dry}) = 77.6\int_{\text{surface}}^{\infty}\frac{P(h)}{T(h)}\,dh \tag{11}$$

Berman (see *Chapter XIII-D*, this volume) has shown that by using the hydrostatic equation

$$dP = -\bar{\rho}g\,dh \tag{12}$$

where $\bar{\rho}$ is the density and g is the gravitational acceleration (assumed constant with altitude), and the perfect gas law

$$P = \bar{\rho}\bar{R}T \tag{13}$$

where $\bar{R}$ is the gas constant, Eq. (11) reduces to

$$\Delta\rho_z^*(\text{dry}) = 77.6\frac{\bar{R}}{g}P_s \tag{14}$$

where P_s is the surface pressure and the * indicates that $\Delta\rho_z$ (dry) has been calculated under certain conditions. Equation (14) predicts a linear correlation between the surface pressure and $\Delta\rho_z$ (dry). To see if this predicted correlation is present, scatter diagrams of $\Delta\rho_z$ versus P_s were plotted and the correlation between them calculated. The results of this process for the Edwards AFB, as illustrated in Fig. 8, always show a high (i.e., > 0.97) correlation between the dry zenith range effect and surface pressure.

The overseas data cannot be used to verify the correlation according to Eq. (14) since the data generally stops below 30,000 ft. However, this correlation may be shown to be present if the upper limit of Eq. (11) is replaced by $h_{\max}$ so that

$$\Delta\rho_z^*\ (\text{dry}, h_{\max}) = 77.6\frac{\bar{R}}{g}[P_s - P(h_{\max})]$$

where $\Delta\rho_z$ (dry, $h_{\max}$) is the zenith range effect produced by the troposphere between the surface and $h_{\max}$.

It is not surprising that correlation between the dry zenith range effect and surface pressure exists because the hydrostatic equation and gas law used to obtain Eq. (14) are very close to the equations used to determine the height of a particular set of weather measurements.

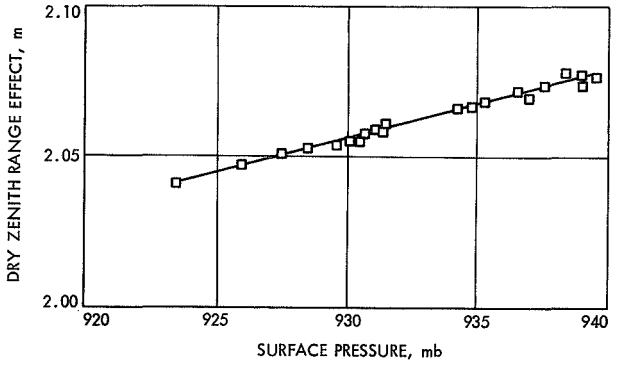

Fig. 8. Scatter diagram showing correlation between dry zenith range effect and surface pressure for data taken over Edwards AFB during March 1967

8. Cursory Examination of Methods for Predicting the Wet Zenith Range Effect From Surface Measurements

From Eqs. (5) and (6) the wet zenith range effect is calculated by evaluating the following integral:

$$\Delta\rho_z\,(\text{wet}) = 2280\int_0^\infty \frac{1}{T^2}\exp_{10}\left[\frac{7.4475(T-273.2)}{T-38.5}\right]R\,dh \tag{15}$$

Obviously, to perform this integral based upon surface measurement, it is necessary to specify some models for $T(h)$ and $R(h)$ based upon these quantities. The difficulty in specifying models that are representative of what the physical situation may actually be lies not with $T(h)$, but almost entirely with $R(h)$. For example, the difference between the representative wet refractivity profiles shown in Fig. 9 is due for the most part to differences in the relative humidity profile. Note that although the March 9 wet surface refractivity is only 70% of the March 10 value, the March 9 $\Delta\rho_z$ (wet) is twice as large as the March 10 value.

Berman (*Chapter XIII-D*, this volume) has made an attempt at determining an equation for $\Delta\rho_z$ (wet) in terms of surface measurements by assuming that the temperature falls off according to a constant lapse rate and the relative humidity is constant at its surface values. Berman's equation for the wet zenith range effect, $\Delta\rho_z(B)$, which results from his assumptions, is given as

$$\Delta\rho_z(B) = \left[\frac{C_1C_2R_s}{\gamma(T_s)}\right]\left[\frac{(1-T_sC)^2}{B-AC}\right]\exp\left[\frac{AT_s-B}{T_s-C}\right] \tag{16}$$

where

$C_1 = 77.6$

$C_2 = 29341.0$

T_s = surface temperature

R_s = surface relative humidity

$A = 7.4475\ \ln(10)$

$B = 2034.28\ \ln(10)$

$C = 38.45$

$$\gamma(T_s) = \frac{T_s - 216.65}{11 - h_0}$$

h_0 = station elevation, km

To see how well Berman's wet model predicts the wet zenith range effects, monthly plots were made with $\Delta\rho_z(B)$ computed from Eq. (16), $\Delta\rho_z$ (wet) computed from the radiosonde balloon measurements, and the difference between them. An example of these plots is shown in Fig. 10.

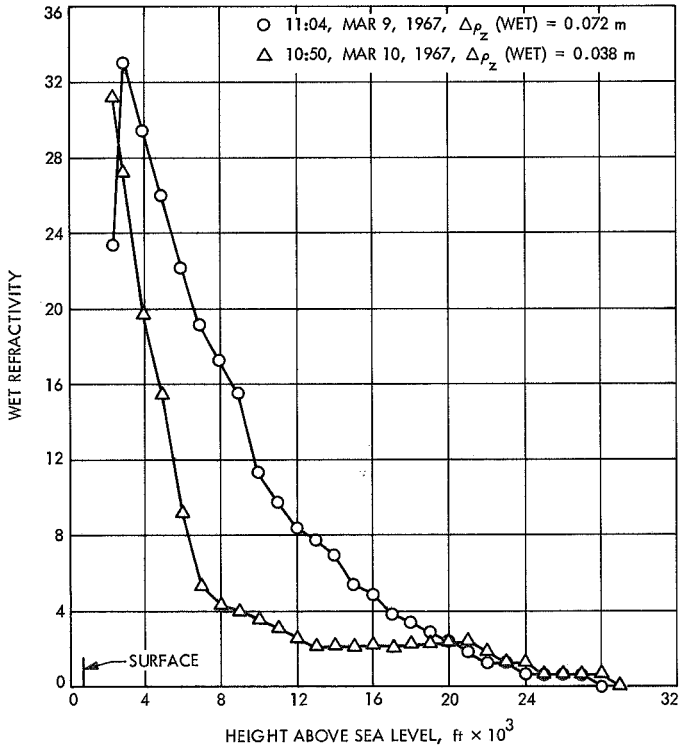

Fig. 9. Wet refractivity profiles over Edwards AFB

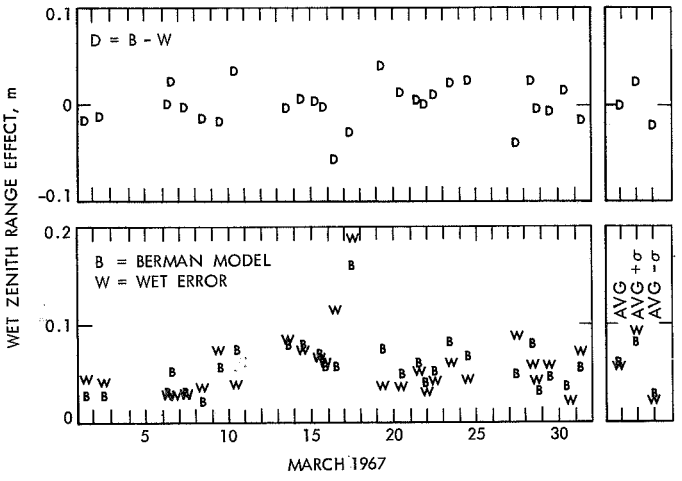

Fig. 10. Actual, predicted, and differenced wet zenith range effect for Edwards AFB during March 1967

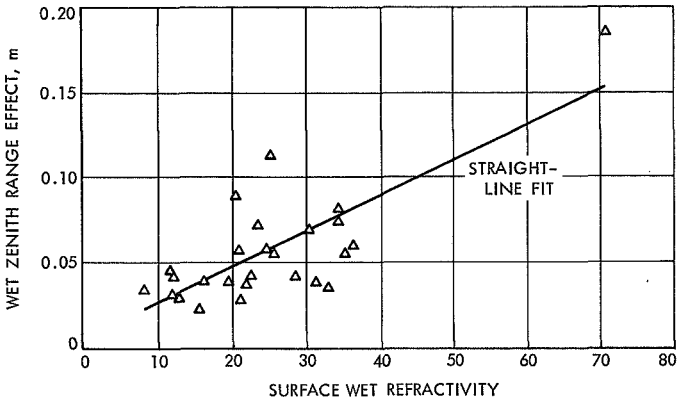

Fig. 11. Surface wet refraction vs wet zenith range effect with correlation 0.76 for Edwards AFB during March 1967

To investigate the correlation between the wet zenith range effect and the wet surface refractivity, the monthly $\Delta\rho_z$ (wet) versus N_w (surface) scatter diagram was plotted, the correlation calculated, and a least-squares straight-line fit made. An example of this output is shown in Fig. 11. Unfortunately, the slope and intercept of this fitted straight line vary widely throughout the year.

A summary of the results of trying to predict $\Delta\rho_z$ (wet) from the Edwards AFB data is given in Fig. 12. This figure is representative of the overseas data and indicates that nothing substantial is gained by using surface measurements and Berman's wet model in its present form. However, if the monthly variations of the average wet zenith range effect are repetitive from year to year, it may be possible to reduce the standard deviations from the yearly average of approximately 0.06 m by a factor of two.

9. Apparent Changes in Station Locations Produced by the Troposphere

For the elevation angles larger than approximately 5 deg, a good (10%) approximation to the range effect at a particular elevation angle, γ, produced by a spherically symmetric troposphere is given by

$$\Delta\rho(\gamma) = \frac{\Delta\rho_z}{\sin\gamma} \tag{17}$$

If the tracking station is viewing a zero-declination spacecraft, the time behavior of the tropospheric range rate correction associated with the above equation will be

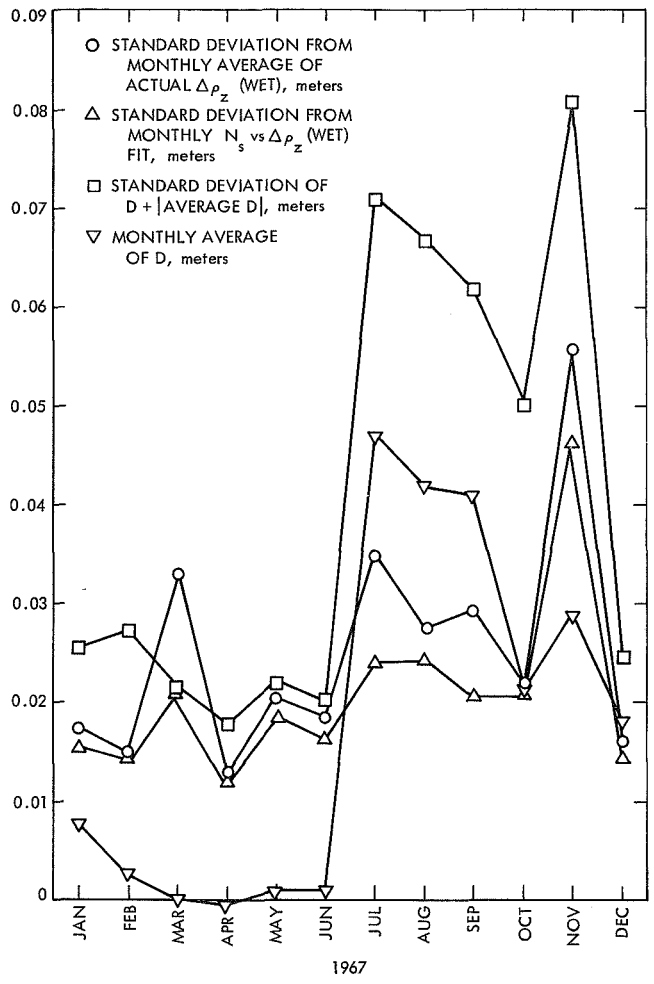

Fig. 12. Monthly summary of wet zenith range effect predicted from surface weather measurements taken at Edwards AFB during 1967

given by

$$\Delta\rho(t) = \frac{\omega\,\Delta\rho_z}{\cos\Phi}\frac{\sin\omega t}{\cos^2\omega t}$$

where

t = time past meridian crossing

ω = angular rotation rate of the earth

Φ = latitude of tracking station

In the previous sections it has been shown that the standard deviation of $\Delta\rho_z$ from a constant model is approximately 0.07 m and if surface pressure measurements are used in conjunction with the dry Berman model this standard is reduced to approximately 0.06 m. An examination of the plots showing $\Delta\rho_z$ as a function of time has

given an estimate that the average of the absolute value of the rate of change of $\Delta\rho_z$ is approximately 0.02 m/day.

A useful artifice for investigating navigational errors, such as the ones produced by the troposphere, is to describe them in terms of equivalent errors in tracking station locations. As described in SPS 37-57, Vol. II, pp. 24–29, an effect which corrupts tracking data can be decomposed into parameters, one of which is the apparent change in the station distance off the spin axis, Δr_s, and another is the apparent change in the station's longitude, $\Delta\lambda$. The results of performing such an analysis for the various unmodeled tropospheric effects discussed above are given in Table 5. The numbers in the table were computed under the assumption that a tracking station situated at a latitude of 0° was viewing a zero-declination spacecraft and taking range rate data throughout a pass which was symmetric about the meridian crossing and had a minimum elevation angle, γ_{min}.

Table 5. Estimated standard deviations of apparent daily change in station locations[a]

Minimum elevation angle, deg	Δr_s, m	$\Delta\lambda$, m
15	0.26	0.12
10	0.42	0.19
5	0.85	0.42

[a]For zero-degree latitude station viewing a zero-declination spacecraft under assumption that $\Delta\rho_z(t) = 0.06$ m + (0.02 m/day)t days.

10. Summary and Conclusion

An examination of radiosonde balloon data taken during 1967 has shown that the tropospheric zenith range effect is quite a stable quantity and will almost always stay within ±5% of its yearly average. The variation produced by the dry constituents can be eliminated almost entirely if use is made of surface pressure measurements. The remaining 80 or 90% of the variations may possibly be reduced up to a factor of two if the seasonal variations of the wet zenith range effect is repeatable over the years. The effects of the zenith range effect upon radio tracking data may be grossly represented by errors in tracking station locations of approximately $\Delta r_s = 0.3$ m and $\Delta\lambda = 0.1$ m if a minimum elevation of 15 deg is used.

These estimates of the navigational errors produced by the variation of the zenith range effect should not be taken to represent the total effect of the troposphere. Unfortunately, there are other possible tropospheric error sources which may contribute significantly to the errors produced by the troposphere. Two such error sources arise from mapping zenith values to arbitrary elevation angles, and from effects produced by the nonhomogeneous structure of the troposphere. These other tropospheric error sources are currently under investigation.

Reference

1. Bean, B. R., and Dutton, E. J., *Radio Meteorology*, National Bureau of Standards, Monograph 92, p. 11, 1966.

C. The Effect of the Diurnal Variation of the Earth's Ionosphere on Interplanetary Navigation, *B. D. Mulhall and K. L. Thuleen*[1]

1. Introduction

The need to calibrate the effect of charged particles in the earth's ionosphere on radio tracking data has been recognized and was undertaken on a research basis for the *Mariner* Mars 1969 encounter.[2] To better understand the effect of the ionosphere on navigation and to predict what the effect might be for future missions, a parametric study was performed. The diurnal variation of the ionosphere was modeled. The seasonal and solar cycle changes in the model parameters were determined by fitting the model to actual ionospheric measurements sampled from different seasons

[1]The authors wish to acknowledge the assistance of S. Finley in developing programs used in this study.

[2]Mulhall, B. D., et al., *Tracking System Analytic Calibration Activities for the Mariner Mars 1969 Mission*, Technical Report 32-1499. Jet Propulsion Laboratory, Pasadena, Calif. (in press).

and years. To represent different mission geometries, the ionospheric effect was computed for various sun–earth–probe angles.

2. Ionospheric Model

The diurnal variation of the charged particle content in the earth's ionosphere can be represented by

$$E_c = \begin{cases} D_c + A_c \cos \omega (t - \Phi) \\ \text{whichever is greater} \\ D_c \end{cases}$$

where

E_c = modeled columnar electron content

ω = rotational rate of the earth

t = meridian time

and D_c, A_c, and Φ are the model parameters.

The model parameters represent the nighttime average electron content, D_c, the peak concentration during the day, $D_c + A_c$, and the time of the peak concentration, Φ. This model has been used for some time in the reduction of Faraday rotation measurements made at Goldstone, and was intended as a scheme for predicting the diurnal variation. However, its prediction capability is limited (Mulhall, SPS 37-64, Vol. II, pp. 25–27).

The model was fitted to measurements of the ionosphere made by Stanford Radio Science Laboratory[3] and by JPL at the Venus site (DSS 13). Figure 1 shows the seasonal variations in the values of D_c and A_c. Table 1 lists the sample mean and standard deviation of each parameter for spring, summer, fall, and winter. From the figure and the table, it can be seen that the nighttime concentrations of charged particles are generally higher in summer than in winter, probably

[3]The authors wish to thank M. Davis and T. Howard of the Center for Radar Astronomy, Stanford Electronics Laboratories, for providing the ionospheric data.

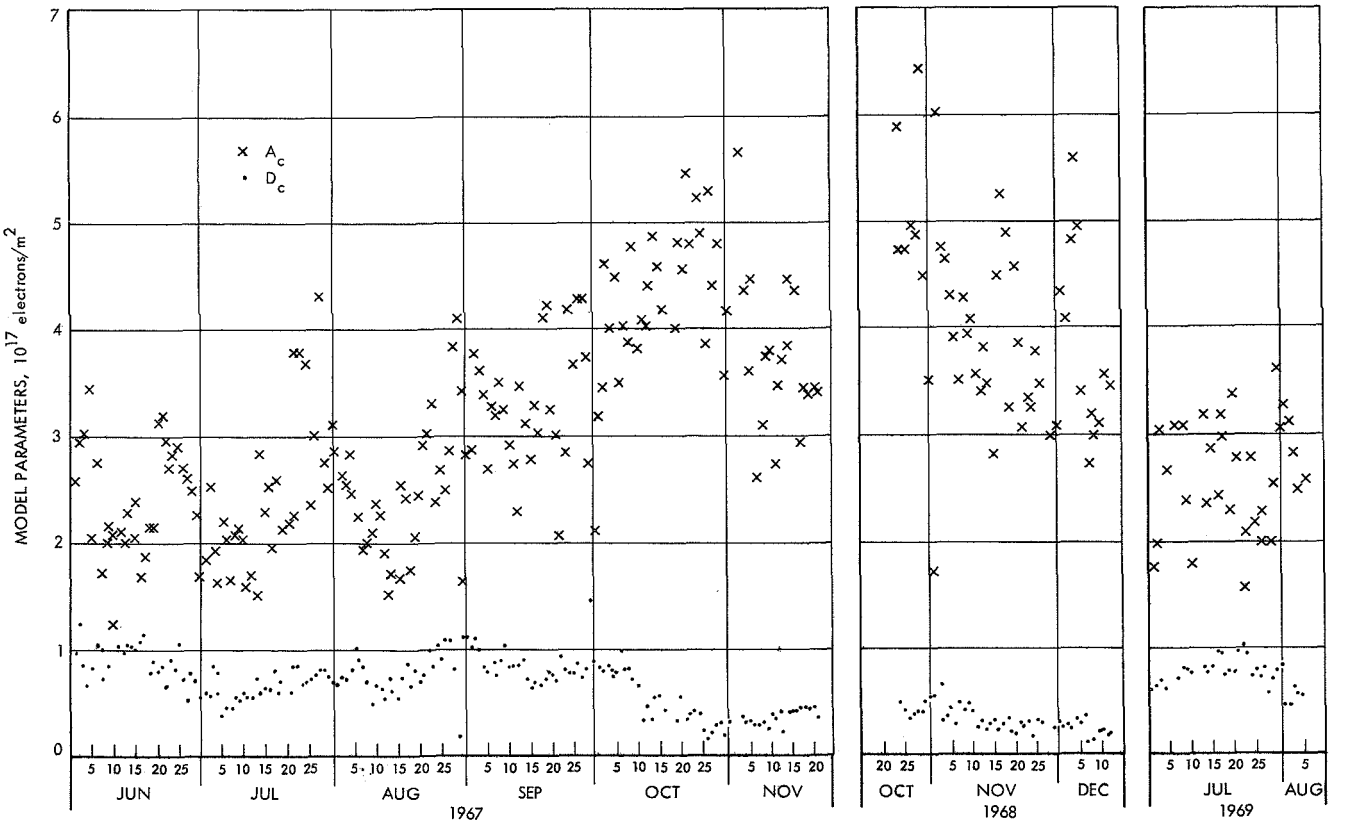

Fig. 1. Ionospheric conditions

Table 1. Seasonal variation of ionospheric model parameters (northern hemisphere)

Parameter	Summer			Spring/Fall		Winter
	1965	1967	1969	1967	1968	1965
A_c						
Mean	1.32	2.44	2.65	3.77	4.06	1.49
Standard deviation	0.09	0.62	0.57	0.79	0.95	0.15
D_c						
Mean	0.39	0.79	0.78	0.60	0.34	0.29
Standard deviation	0.14	0.23	0.15	0.27	0.11	0.15
Φ, hours						
Mean	13.17	13.90	13.03	13.79	12.61	12.93
Standard deviation	2.38	1.82	2.18	1.52	1.48	1.51
Number of days in sample	27	90	32	78	48	32

due to the warmer nighttime temperatures. However, daytime peak concentrations are higher in fall, winter, and spring than in summer. There are several theories proposed to explain this seemingly contradictory situation; however, none has been completely satisfactory. The uncertainty in Φ (see Table 1) increases in summer and, as discussed in SPS 37-64, Vol. II, the summer ionosphere stays at a maximum concentration for a fairly long period of time.

The 11-yr solar cycle reached a maximum in 1968. By comparing the average values of nighttime and daytime peak concentrations (D_c and A_c) listed in Table 1 and Fig. 1 for 1965 versus the values for 1967, 1968, and 1969, it can be seen that electron concentrations tend to increase with the solar cycle.

3. Navigational Effect

To determine the ionospheric effect on navigation for various missions, the sun–earth–probe angle (χ) was varied as the parameters of the model were varied. By using the three-parameter navigation filter developed by Hamilton and Melbourne (reference footnote 2; SPS 37-39, Vol. III, pp. 18–23; and SPS 37-57, Vol. II, pp. 24–29), the ionospheric effect was resolved into apparent changes in the tracking station longitude, the station distance from the earth's spin axis, and changes in apparent spacecraft range rate:

$$\dot{\rho} = a + b \sin \omega t + c \cos \omega t$$

where

$$a = \dot{r}$$

$$b = r_s \omega \cos \delta$$

$$c = r_s \omega \Delta\theta \cos \delta$$

and

$\dot{\rho}$ = spacecraft station range rate

$\dot{r}$ = spacecraft geocentric range rate

r_s = tracking station spin radius

δ = spacecraft declination

and $\Delta\theta$ can be considered the error in tracking station longitude.

Using the program ION (reference footnote 2), doppler effects of the ionosphere were computed for various sun–earth–probe angles. The doppler effects were fitted to the three-parameter navigation filter by least-squares estimation. The empirical sensitivities of a, b, and c with respect to A_c, D_c, and Φ were computed. Figures 2 and 3 show the partial derivatives of a, b, and c with respect to A_c and D_c. Figures 4, 5, and 6 show the partial derivatives of a, b, and c with respect to Φ for various values of Φ since these partials are nonlinear.

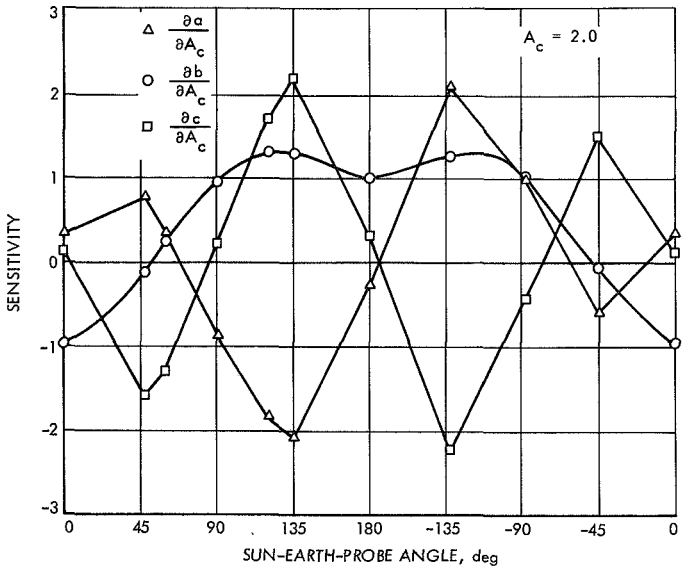

Fig. 2. Sensitivity of a, b, c with respect to A_c versus sun–earth–probe angle

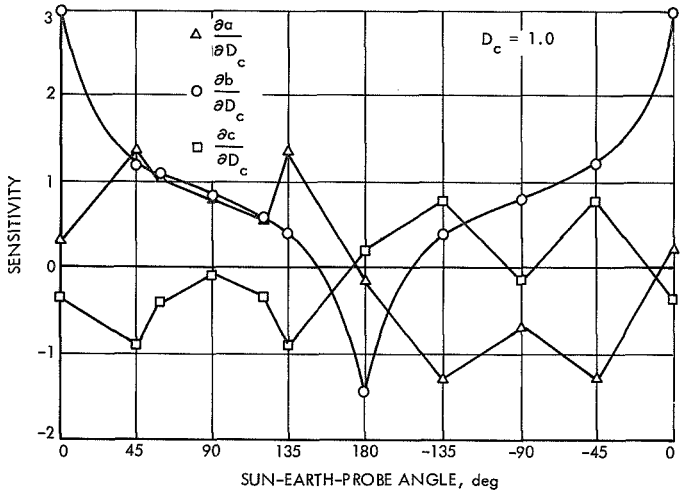

Fig. 3. Sensitivity of *a*, *b*, *c* with respect to D_c versus sun–earth–probe angle

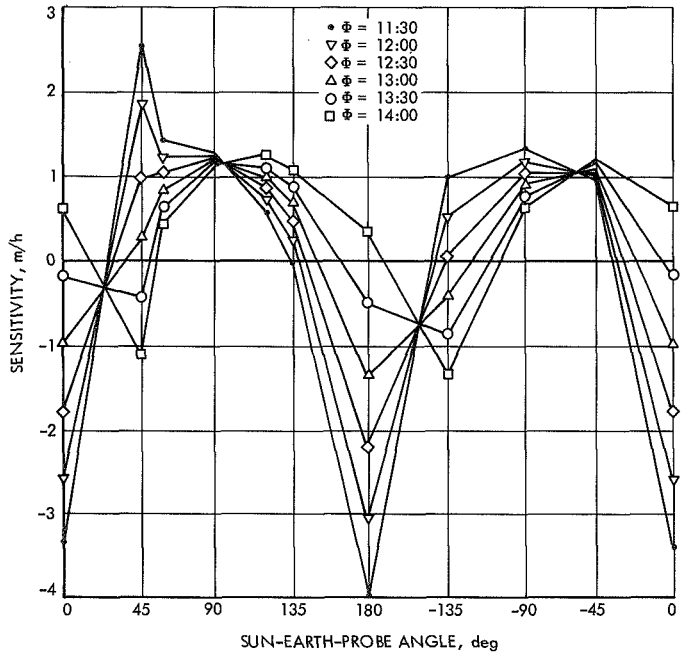

Fig. 4. Sensitivity of *a* with respect to Φ versus sun–earth–probe angle

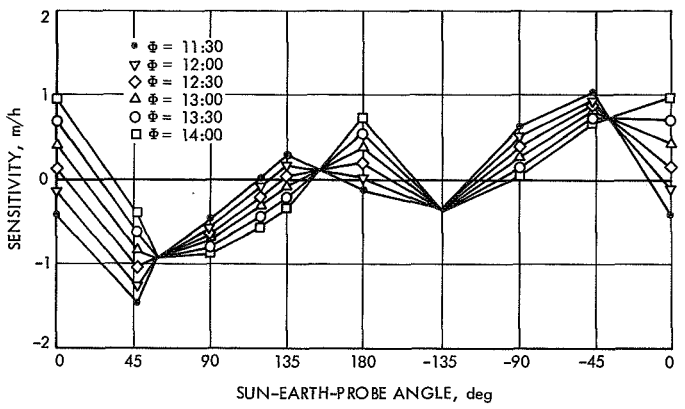

Fig. 5. Sensitivity of *b* with respect to Φ versus sun–earth–probe angle

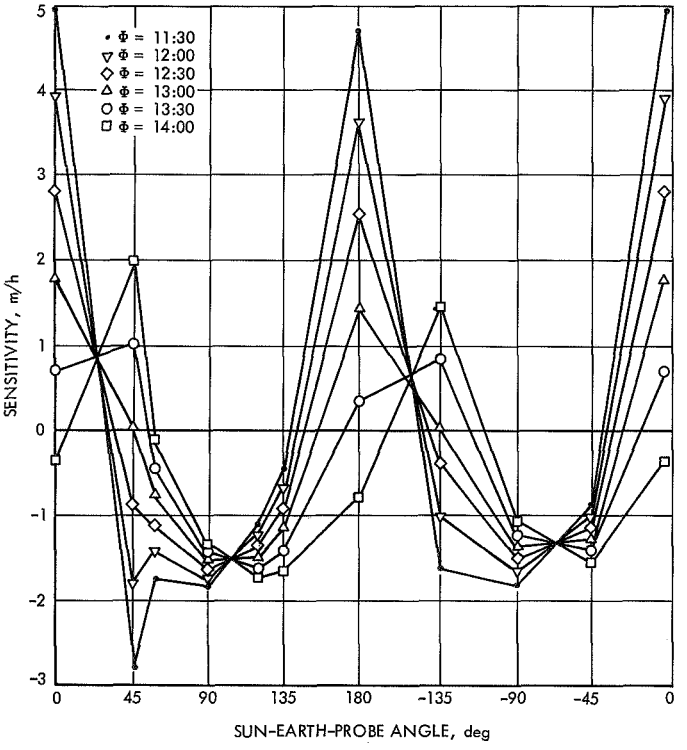

Fig. 6. Sensitivity of *c* with respect to Φ versus sun–earth–probe angle

The high negative correlation between *a* and *c* is apparent in these figures. A radical change in *a* is accompanied by an opposite and nearly equal change in *c*. An interesting comparison, which will be performed later, will be to compute the partials for the eigenvalues of *a* and *c*. Presumably, these will resemble the more smoothly varying partials of *b*, since *b* is independent of *a* and *c*.

4. Estimation of Ionospheric Effect on Navigation

The intended use of the partial derivative is to estimate the sensitivity of orbit determination to ionospheric effects. The sun–earth–probe angle (χ) at critical mission phases characterized the ionospheric effect since the relationship of the spacecraft rise and set times to the diurnal variation of the ionosphere is typified by χ. For

example, the effect of the ionosphere on b (and, consequently, on r_s or spacecraft declination) with respect to the amplitude of the peak electron concentration (A_c) is at a maximum at $\chi = 120$ deg. *Mariner VI* encounter occurred in late July 1969 at about a sun–earth–probe angle of 120 deg. In July 1967, χ for *Mariner V* was approximately 15 deg. The average ionospheric effect on r_s for the month of July for *Mariner VI* was 3.3 m while for *Mariner V* the effect was 1.1 m. Even though the ionospheric concentrations of electrons were similar during July 1967 and July 1969, the increased sensitivity of b due to χ caused an increased navigational error.